# Concentric Precurved Bellows: New Bending Actuators for Soft Robots

Jake A. Childs and Caleb Rucker

Abstract—We present a new mechanical bending actuator for soft and continuum robots based on a pair of concentric precurved bellows. Each bellows is rotated axially at its base, allowing independent control of the curvature and bending plane of the concentric bellows pair. Rotation of precurved nested tubes is a well-known principle by which needle-sized concentric-tube robots operate, but the concept has never been scaled up to large diameters due to the trade-offs of increased actuation forces, decreased range of motion, strain limits, and torsional windup. In this letter, we show that using bellows structures instead of tubes allows two important breakthroughs: (1) actuation by rotation of precurved concentric elements can be achieved at much larger scales, and (2) torsional lag (i.e. when the relative tube angle at the tip differs from that at the base) and torsional instability are virtually eliminated due to the high ratio of torsional rigidity to flexural rigidity endowed by the bellows geometry. We discuss the development of two types of 3D printed concentric precurved bellows prototypes (revolute and helical), perform model parameter identification, and experimentally verify a torsionless mechanics model which accounts for direction-dependent rigidities.

Index Terms—Soft Robot Materials and Design; Modeling, Control, and Learning for Soft Robots

# I. INTRODUCTION

OFT and continuum robots have shown great promise for a variety of applications [1]–[3]. As reviewed in [4] and [5], these robots can be actuated by a variety of actuation schemes, which could broadly be categorized as either fluidic (e.g. pneumatic and hydraulic [6]), mechanical (e.g. tendons/cables, push-pull rods, and concentric precurved tubes [7], [8]) or material-based (e.g. piezo-electric, electroactive polymers, [9]). Almost all of these actuation strategies have been employed across a wide range of applications and physical scales, from surgical tools with diameters less than a few millimeters to arms greater than ten centimeters in diameter [7]. However, the actuation paradigm of rotating precurved concentric tubes has so far been notably absent from the development of larger-scale soft or continuum robots. Typical concentric tube robots use relatively "hard" materials

Manuscript received: August 5, 2019; Revised November, 11, 2019; Accepted January 6, 2020.

This paper was recommended for publication by Editor Kyu-Jin Cho upon evaluation of the Associate Editor and Reviewers' comments. This material is based upon work supported by the National Science Foundation under IIS-1652588 (A CAREER Award).

J. A. Childs and D. C. Rucker are with the Department of Mechanical, Aerospace, and Biomedical Engineering, University of Tennessee, Knoxville, TN (e-mail: jchilds3@vols.utk.edu; caleb.rucker@utk.edu).

This paper has supplementary downloadable material available at http://ieeexplore.ieee.org, provided by the authors. This includes one multimedia mp4 format video, which shows concentric precurved bellows assembly, actuation and application. This material is 17.3 MB in size.

Digital Object Identifier (DOI): see top of this page.

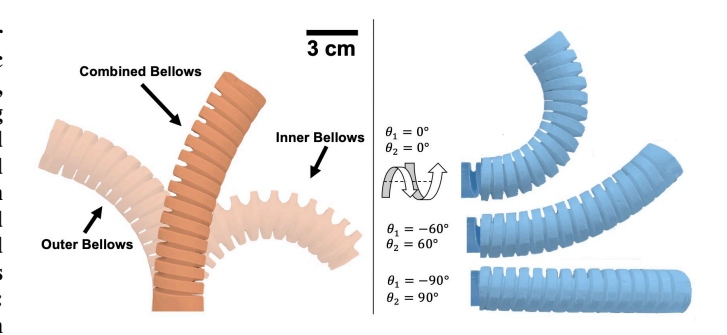


Fig. 1. The equilibrium curvature for a pair of concentric bellows is determined by the precurvature and flexural rigidity of each bellows (left). The concentric bellows pair is actuated by axially rotating the base of each individual bellows. Rotating equal amounts in opposite directions changes the bending angle in a single plane, while rotating equal amounts in the same direction changes the plane of bending. Torsional rigidity is high relative to flexural rigidity due to the bellows geometry, such that a torsionally rigid modeling assumption is accurate.

such as Nitinol (although slightly larger and softer concentric tube robots have been made through 3D printing with semiflexible materials [10]) and have diameters of a couple of millimeters at most. One reason for this is that bending range of tubes decreases at large diameters (less slender aspect ratios) due to material strain limits. Another reason is that the flexural rigidity of solid tubes increases rapidly with diameter, thus requiring much larger actuation torques to rotate the precurved tube bases and bend the tubes. Finally, torsional flexibility and frictional hysteresis continue to be difficult aspects of concentric-tube actuation regardless of robot size. Torsional flexibility can introduce undesired complexities into the behavior of these robots, including non-constant curvature shapes and "snapping" behavior in which the robot can rapidly release stored elastic energy and transition to a different configuration [11], [12]. Torsional flexibility also allows static friction to affect the robot configuration in a hysteretic way, further complicating modeling and control [13], [14].

A key design parameter affecting the behavior of concentric precurved tubes is the ratio of effective flexural rigidity, EI, to effective torsional rigidity, GJ which we refer to as the ratio EI/GJ throughout this paper (where E is Young's modulus, I is the cross sectional second moment of area, G is the shear modulus, and J is the polar moment of area). Lowering this ratio can mitigate or eliminate undesired torsional effects. Cutting a pattern of notches into the tubes (i.e. "patterning") can reduce the effective flexural to torsional rigidity ratio, and a variety of notch patterns have been investigated [15]–[18]. As shown in Table I, while solid tubes have a ratio of around 1.3 (assuming Poisson's ratio  $\nu=1.3$ ), the various notch

TABLE I FLEXURAL TO TORSIONAL RIGIDITY RATIOS

Reference	Design	EI/GJ
_	Solid Tube	1.3 (if $\nu = 0.3$ )
[15]	Horizontal Notches (120°)	0.4
[16]	Horizontal Notches	0.48
[17]	Horizontal Notches (120°)	0.344 to 0.587
[18]	Cellular Hole Pattern	0.94
This Paper	Bellows Tube	0.016 to 0.078

patterning strategies in the works cited above created tubes with EI/GJ ratios ranging from 0.344 to 0.95.

# A. Concept and Contributions

In this paper, we propose to address two existing limitations of the concentric-tube actuation paradigm: (1) small diameter limitations, and (2) torsional compliance limitations, by investigating a new concept for bending actuators for soft and continuum robots based on precurved concentric bellows. While bellows structures are often used as flexible pressure vessels for fluidic actuation strategies [1], we propose to instead use a bellows tube itself as a mechanical transmission element by pre-curving two separate bellows, nesting them concentrically, and then independently rotating their bases in a manner similar to precurved concentric-tube robots. Then, as shown in Figure 1, a range of bending angles in a single plane can be achieved by rotating the two bellows bases by the same angle in opposite directions, if the bellows have equal flexural rigidities. The plane of bending can be changed by rotating the bellows bases equal amounts in the same direction. We will show that the geometry of typical convolution bellows designs exhibits high torsional rigidity relative to flexural rigidity which virtually eliminates negative effects associated with torsion. As recorded in Tables I and III, our prototype bellows tubes exhibited experimental EI/GJvalues between 0.016 and 0.078, which is (1) an order of magnitude lower than typical EI/GJ values achieved so far through laser machined cutout patterns, and (2) low enough to effectively eliminate any torsional lag during actuation, such that simple torsionally rigid kinematic models become accurate. In addition, the bellows concept exhibits a large bending range of motion within reasonable material strain limits. This enables the fabrication of large diameter robots and allows for large precurvatures relative to the bellows diameter. One trade-off is that bellows geometry is not as compact as thin-walled tubes since the bellows convolutions alternate between two different inner and outer diameters, and it may be challenging to scale the concentric-bellows concept down to extremely small diameters. But for larger, soft robotics applications the concentric bellows is a new alternative to other methods such as tendon-based, or fluidic actuation. One potential benefit is that in contrast to tendon-driven robots, friction does not affect the shape much, even at large bending angles. Reliability, safety, and precision are also benefits, due to the simple mechanical nature of the actuation.

In this letter, we detail the design and fabrication of 3D printed pairs of precurved concentric bellows. We demonstrate parameter identification through FEA and experimental tests, and we extend the torsionally rigid concentric-tube kinematic

model originally developed in [11] to handle the possibility of direction-dependent flexural rigidities. Finally, we experimentally confirm torsionally rigid behavior during concentrictube actuation, and validate model shape accuracy for bending angles up to 120°.

#### II. BELLOWS FABRICATION AND DESIGN

In this section, we demonstrate low-cost methods for additive manufacturing of concentric bellows pairs through 3D printing (fused-deposition modeling), suitable for research and the rapid iterative development of soft robot actuators.

## A. Convolution Design

A typical bellows design consists of a convolution geometry (Figure 2 (a)) that is revolved around a central axis to form a "revolute bellows." For 3D printing, we use a v-shaped inner geometry and a flat outer geometry, as shown in Figure 2, to minimize overhangs and provide a stable interface with the print bed. The plate width (the difference between a bellows inner and outer radii) and the wall thickness are the dominant factors in influencing the flexural rigidity, while the overall diameter is relatively less significant (in contrast to solid tubes). This enables an inner/outer balanced stiffness pair of bellows [12] to be designed. In our example design as shown in Figure 2, the inner bellows is just slightly stiffer than the outer because it has a smaller plate width and the same wall thickness.

## B. Revolute Bellows

Revolving an inner and outer convolution geometry about a central axis results in a concentric pair of revolute bellows that cannot be assembled or disassembled because they are interlocked. One way to construct such an assembly is to additively manufacture the two bellows tubes simultaneously in the assembled (interlocked) state, as shown in Figure 2 (b). While dissolvable support material can be used to support and separate the two bellows surfaces during printing, it is very challenging to subsequently dissolve the support material due to the winding convolution geometry and small clearance between the parts. To avoid this difficulty, an extruded cut, which makes an angle  $\mu$  from the outer tangent, can be applied to either side of the assembled bellows CAD model as shown in Figure 2 (b). The geometry of each individual bellows can then be independently anchored to the build plate, and the pair can be printed in the assembled state without support material.

# C. Helical Bellows

It is also possible to create a bellows tube geometry by specifying a helical extrusion of the convolution geometry (with pitch h) instead of a revolved extrusion. This allows easy assembly and disassembly of a bellows tube pair by simply threading them into or out of each other. Thus, individual helical bellows can be printed and precurved separately and subsequently assembled. Actuation of a helical bellows pair is then achieved by combined translation and rotation of each base with pitch h.

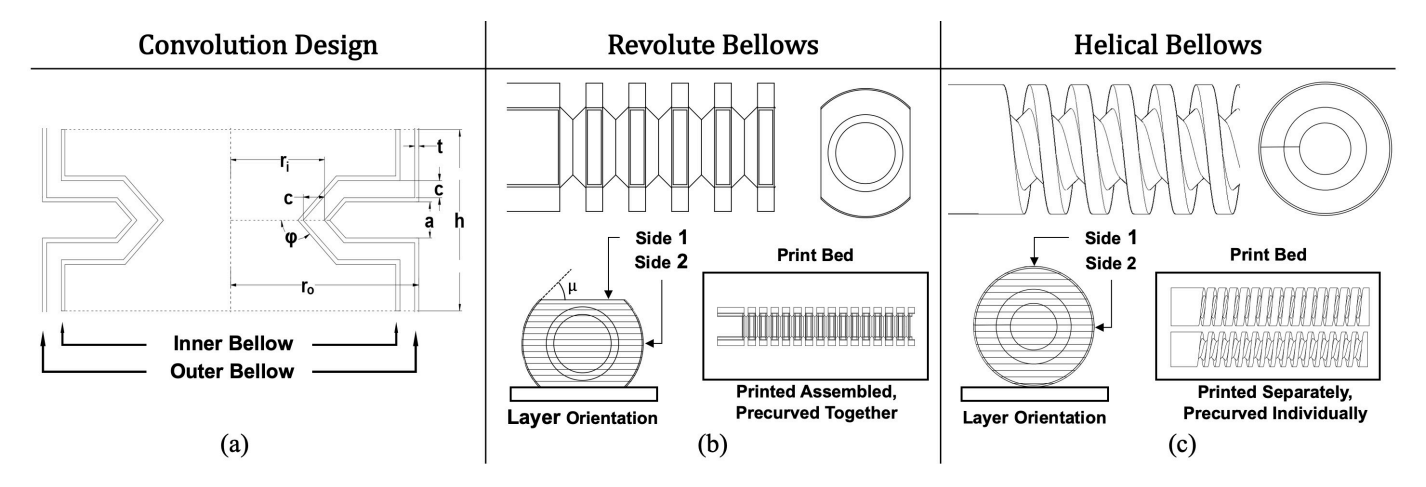


Fig. 2. Convolution geometry schematic and design parameters (a) used for revolute (b) and helical bellows (c). 3D printing layer orientation along with side references used in parameter estimation and kinematic experiments are shown for both bellows. A revolute bellows pair cannot be disassembled and must be printed and precurved in the assembled state. Helical bellows can be printed and precurved separately and subsequently assembled.

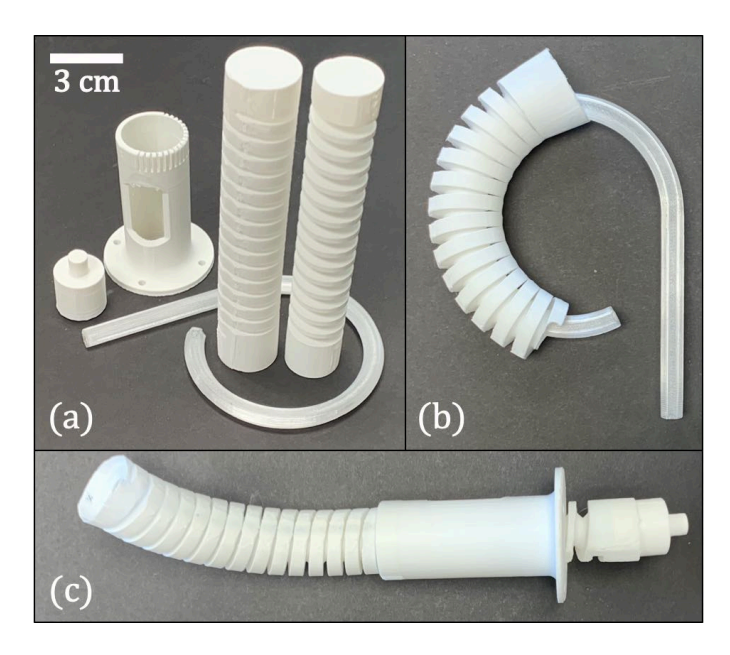


Fig. 3. Components used to fabricate a pair of helical precurved concentric bellows (a). The curvature jig is inserted through the inner lumen of the bellows and enforces the new shape onto the bellows in the precurving process (b). Once precurved, inner and outer bellows attachments can be used to mount bellows onto actuation systems (c).

# D. Pre-Curving via Heat Treatment

After either a revolute bellows pair or an individual helical bellows is printed, the bellows can be pre-curved by constraining it to a desired shape via a jig and heating it to the glass transition temperature of the material. After glass transition, the part is allowed to cool in its fixtured precurved state and is subsequently removed. We note that it is also possible to eliminate the heat treatment step by simply printing the concentric bellows pair in the pre-curved state, but this requires much more effort and complexity in the CAD modeling of the design, whereas an uncurved bellows design is very straightforward to generate.

TABLE II
BELLOWS DIMENSIONS OF 3D PRINTED PROTOTYPE USED IN KINEMATIC
AND BENDING EXPERIMENTS

Parameter	Value
Inner radius, $r_i$	7.5 mm
Outer radius, $r_o$	15 mm
Wall thickness, t	0.3 mm
Clearance, c	1.2 mm
Convolution pitch, h	9 mm
Convolution gap, a	2.5 mm
Inner convolution angle, $\varphi$	135°
Tangent angle at cut, $\mu$	45°

# E. Example Bellows Specifications and Fabrication

The dimensions of the bellows prototypes for both revolute and helical designs used in our experiments are tabulated in Table II. These dimensions were selected iteratively such that bellows could smoothly rotate within one another and feasibly be fabricated. Prototypes were 3D printed out of PLA on a Makerbot Replicator 2 at 230°C and a layer height of 0.15 mm. Single wall (shell) print settings with no infill and a floor/ceiling height of 0.4 mm were used to achieve a finished part with roughly uniform wall thickness. We inserted a curvature jig through the bellows inner lumen to enforce a desired precurvature on the bellows as shown in Figure 3 (b). To ensure jig shape is maintained through the heating process the jigs were 3D printed using a co-polyester material (ColorFabb HT) with a higher glass-transition temperature greater than the bellows material (PLA). The jig-constrained bellows were placed in an oven (Quincy Lab Model 10 Oven) at 60°C for 20 minutes. After heating, the bellows were ambiently cooled to room temperature (approx. 24°C) while leaving the curved jig within the bellows for at least 20 minutes. After removal of the jig, the inner and outer precurved bellows are each connected to a drive mechanism, shown in Figure 3 (c), which allows coupling to a manual actuation system which axially rotates and translates their bases, as detailed in Section V.

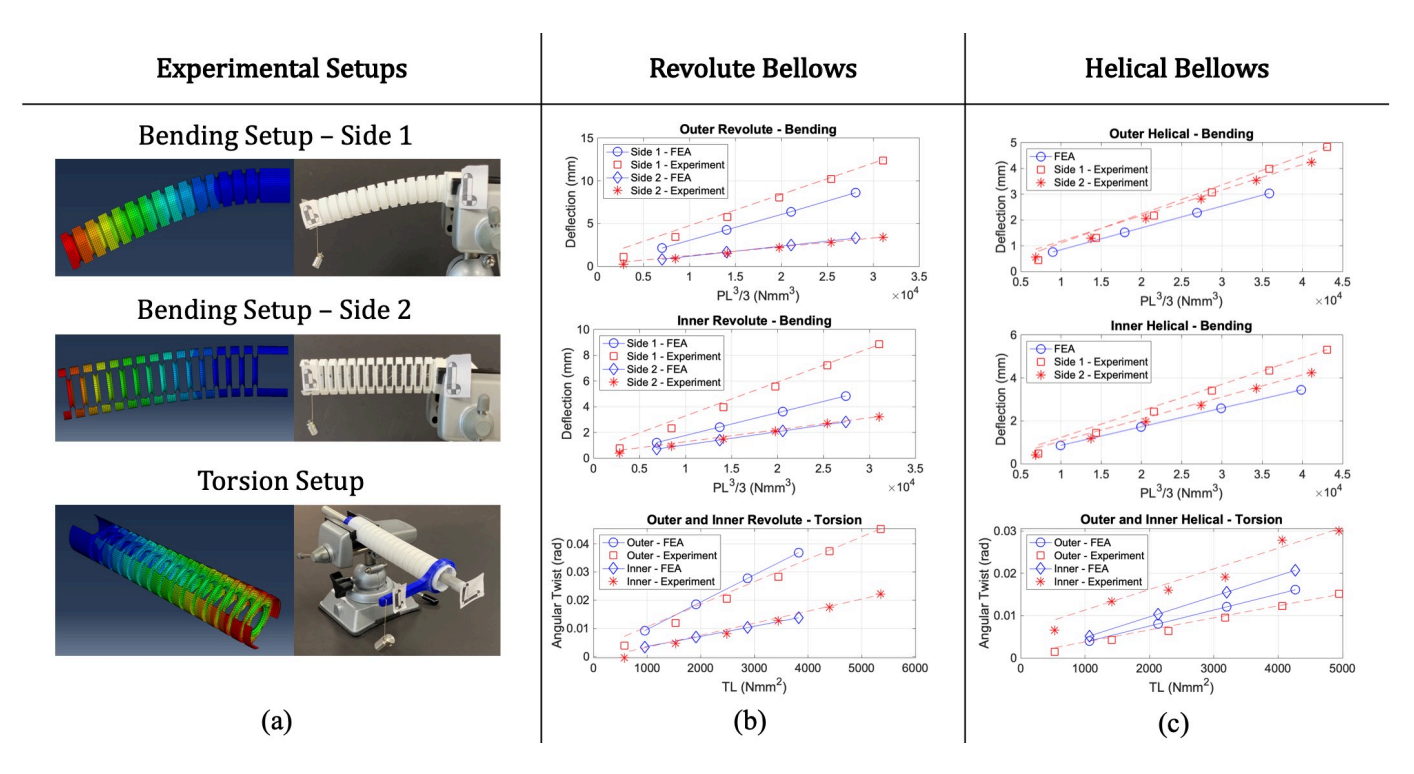


Fig. 4. Results of bellows parameter characterization experiments. The FEA and experimental setups are shown in (a) with the bending and torsion results for the inner and outer bellows for the revolute (b) and helical (c) designs.

# III. PARAMETER CALIBRATION

In order to develop accurate kinematic models and predict concentric-tube manipulator performance, it is necessary to calibrate the effective flexural and torsional rigidities of a bellows design. In this section, we calibrate these model parameters for our prototype bellows by fitting the rigidity parameters to deflection data from small-deflection loading scenarios. We compare calibrations using data from (1) FEA simulations of the bellows, and (2) experimental tests on the physical prototypes. These parameters are ultimately used in a constant-curvature kinematic model in the next section.

# A. Calibration Setups

The FEA simulations were produced using Abaqus/Standard (Simulia, Dassault Systems). Each bellows design was modeled using quadrilateral shell elements (element type S4R) with a thickness of 0.3 mm. Young's modulus for 3D printed PLA can vary between 1.8 to 3.3 GPa based on a variety of material factors and testing standards [19]. For our FEA simulations we used a Young's modulus of 3.15 GPa which is reported in the data sheet of a commonly used PLA (Ultimaker) [20]. Typical simulation run time was around 10 seconds. The experimental setup used a stereoscopic camera (ClaroNav MicronTracker H3-60) and markers attached to the bellows prototypes to measure tip deflections and rotations from bending and torsion experiments as show in Figure 4 (a).

# B. Fitting the Flexural Rigidity

To determine the effective flexural rigidity, we apply a range of tip loads at the distal bellows end and measure the

TABLE III PARAMETERS IDENTIFIED FROM FEA AND EXPERIMENTAL MEASUREMENTS FOR REVOLUTE AND HELICAL BELLOWS

		EI (Nm²)		GJ (Nm <sup>2</sup> )		EI/GJ		
Bellow Type		Side	FEA	Experiment	FEA	Experiment	FEA	Experiment
	Outer	Side 1	0.0032	0.0025	0.104	0.115	0.031	0.022
Revolute -		Side 2	0.0085	0.0090			0.082	0.078
	Inner	Side 1	0.0057	0.0035	0.235	0.215	0.024	0.016
		Side 2	0.0097	0.0097			0.041	0.045
Helical —	Outer	Side 1	0.0118	0.0081	0.300	0.322	0.039	0.025
		Side 2	0.0118	0.0093			0.039	0.029
	Inner	Side 1	0.0101	0.0074	0.168	0.172	0.060	0.043
		Side 2	0.0101	0.0089			0.060	0.052

deflection. The max tip load is 5 grams in order to remain in the small deflection range. We then fit the effective flexural rigidity EI to the small deflection data using the Euler-Bernoulli tip deflection formula.

$$w = \frac{PL^3}{3EI} \tag{1}$$

where w is the tip deflection, P is the tip load, and L is the length of the beam. We plot the deflection data and the linear fit in Figure 4. In the FEA trials, tip masses of 1, 2, 3, and 4 grams are applied to the distal end while the experimental trials include an additional 5 gram load as well as the mass of the tip marker. We performed these trials with loads applied in the direction of Sides 1 and 2 for both the revolute and helical designs detailed in Section II. After linearly fitting the

5

deflection data versus  $PL^3/3$  (as outlined in ASTM testing standards [21]), the slope of this fitted line then corresponds to 1/EI, the inverse of the estimated flexural rigidity. The linear fit R-squared values for all flexural rigidity trials were at least 0.99 or greater.

#### C. Fitting Torsional Rigidity

The effective torsional rigidity GJ can be estimated by measuring the angular twist of the bellows  $\phi$  from an applied torsional load T to a bellows of length L. The twist angle can be calculated as follows:

$$\phi = \frac{TL}{GI} \tag{2}$$

We plot angular twist  $\phi$  versus TL in Figure 4 and perform a linear fit of the FEA angular twist and the experimental angular twist data. The slope of these fitted lines then correspond to 1/GJ, the inverse of the effective torsional rigidity.

In the physical experiment, an arm is rigidly attached to each bellows as shown in Figure 4 (a). Masses of 10, 20, 30, 40, and 50 grams were placed at the end of the arm which is 75 mm in length from the centerline of the bellows to the location of the loading mass. An aluminum tube was inserted through the center of each bellows prototype to eliminate bending. The FEA trials use a similar loading condition where moments of 0.0074, 0.0147, 0.0221, 0.0294 Nm were applied. The R-squared values for all torsional rigidity trials were greater than 0.97. The results for these loading cases are shown in Figure 4 (b) and (c).

# D. Calibration Results

Results of parameter characterization are compiled in Table III. In general, FEA predicted slightly stiffer flexural rigidity values and slightly less stiff torsional rigidity values than those that were experimentally determined. Experimentally determined EI values for side 1 of each design were expected to be lower since 3D printed parts typically have a lower flexural rigidity in the direction of print orientation, due to layer effects [19]. Considering the uncertainties in 3D printed wall thickness, the range of uncertainty in Young's modulus, and the complexity of bellows geometry, FEA predicted reasonable bending and torsional rigidity values. We note that even though there is some error in the FEA predicted parameters, the accuracy is sufficient for using FEA as an initial design tool, while the more accurate experimentally calibrated parameters can be used for kinematic prediction and control, as we do in Section V.

The EI/GJ ratios from the physical experiments ranged from 0.016 to 0.078 which is an order of magnitude lower than previous methods for reducing this ratio based on laser cutting notches into metal tubes as listed in Table I. As we will experimentally show in Section V, ratios this small can be considered effectively zero because they produce a concentric tube robot exhibiting no torsional deformation or lag between the proximal and distal ends (i.e. actuator angles are transmitted down the length without loss, even to friction). Thus, we can reasonably use kinematic models that assume infinite torsional rigidity.

# IV. KINEMATIC MODELING

In this section, we generalize a prior torsionally-rigid concentric-tube kinematic modeling framework [11] to account for concentric structures that can exhibit direction-dependent flexural rigidity (such as 3D printed bellows as demonstrated in the previous section). This is a straightforward advancement, but we are not aware of any prior concentric-tube model that includes this feature.

Let  $\mathbf{m}_i = [m_x \ m_y]^{\top} \in \mathbb{R}^2$  be the vector of the internal bending moment (about the x and y cross-sectional axes) carried by the  $i^{th}$  bellows expressed in a material reference frame attached to the  $i^{th}$  bellows. Let  $\theta_i$  be the angle relating the material frame of the  $i^{th}$  bellows to a common robot "backbone" reference frame (defined as a "Bishop frame" that is fixed at the robot base and slides along the backbone without torsional rotation [22], [12]). Assuming zero torsional deformation along the length of the bellows,  $\theta_i$  is constant and equal to the axial rotation of the  $i^{th}$  bellows at its base. Then, a moment balance on a segment of n concentric bellows expressed in the common backbone frame yields

$$\sum_{i=1}^{n} \mathbf{R}(\theta_i) \mathbf{m}_i = \mathbf{0}, \text{ where}$$

$$\mathbf{R}(\theta_i) = \begin{bmatrix} \cos(\theta_i) & -\sin(\theta_i) \\ \sin(\theta_i) & \cos(\theta_i) \end{bmatrix}$$
(3)

A linearly elastic constitutive law relates the internal bending moment to the change in curvature of each bellows as

$$\mathbf{m}_{i} = \begin{bmatrix} EI_{xx,i} & 0\\ 0 & EI_{yy,i} \end{bmatrix} \begin{pmatrix} \begin{bmatrix} u_{x,i}\\ u_{y,i} \end{bmatrix} - \begin{bmatrix} u_{x,i}^{*}\\ u_{y,i}^{*} \end{bmatrix} \end{pmatrix}$$

$$= \mathbf{K}_{i}(\mathbf{u}_{i} - \mathbf{u}_{i}^{*})$$
(4)

where  $\mathbf{K}_i$  is the bending stiffness matrix,  $\mathbf{u}_i$  is the curvature vector containing the precurvature components about the bellows' own x and y cross-sectional axes, and  $\mathbf{u}_i^*$  is the initial precurvature vector of each bellows. Note that the flexural rigidities within  $\mathbf{K}_i$  are allowed to be different in the x and y direction. The equilibrium curvature components in the robot backbone frame are then expressed as

$$\mathbf{u} = [u_x, u_y]^{\top} = \mathbf{R}(\theta_i)\mathbf{u}_i \quad \forall i$$
 (5)

since the bellows must share a common curvature when expressed in the same reference frame. By substituting this into (4), the result can be manipulated to obtain the equilibrium curvature vector,

$$\mathbf{u} = \left(\sum_{i=1}^{n} \mathbf{R}(\theta_i) \mathbf{K}_i \mathbf{R}^{\top}(\theta_i)\right)^{-1} \sum_{i=1}^{n} \mathbf{R}(\theta_i) \mathbf{K}_i \mathbf{u}_i^*.$$
(6)

The constant-curvature transformation matrix T(s) of the robot backbone frame along the arc-length s of a segment

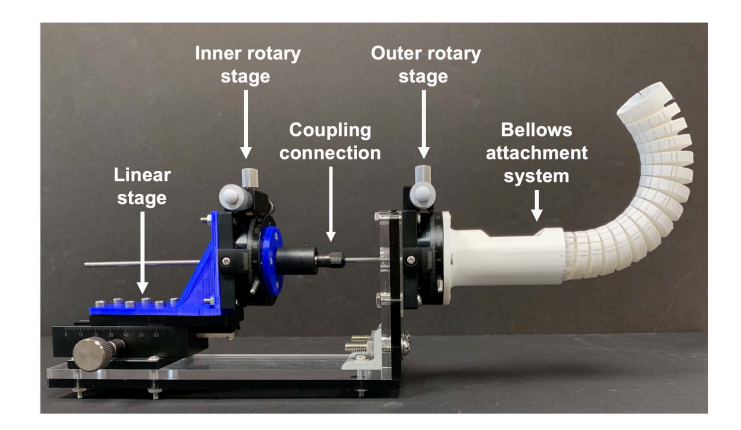


Fig. 5. Manual actuation setup used in model validation experiments. The system provides rotation for both the inner and outer bellows and allows translation of inner bellows.

of overlapped bellows tubes with respect to its base is then computed as

$$\mathbf{T}(s) = e^{\hat{\xi}s} = \begin{bmatrix} \mathbf{R} & \mathbf{p} \\ \mathbf{0}^{\top} & 1 \end{bmatrix}, \text{ where } \hat{\xi} = \begin{bmatrix} 0 & 0 & u_{y} & 0 \\ 0 & 0 & -u_{x} & 0 \\ -u_{y} & u_{x} & 0 & 1 \\ -u_{y} & u_{x} & 0 & 1 \\ 0 & 0 & 0 & 0 & 0 \end{bmatrix}$$

$$\mathbf{R}(s) = \begin{bmatrix} \frac{u_{x}^{2} + u_{y}^{2} C_{\beta}}{U^{2}} & \frac{u_{x} u_{y} (1 - C_{\beta})}{U^{2}} & \frac{u_{y} S_{\beta}}{U} \\ \frac{u_{x} u_{y} (1 - C_{\beta})}{U^{2}} & \frac{u_{y}^{2} + u_{x}^{2} C_{\beta}}{U} & -\frac{u_{x} S_{\beta}}{U} \\ \frac{u_{x} S_{\beta}}{U} & C_{\beta} \end{bmatrix}$$
(7)
$$\mathbf{p}(s) = \begin{bmatrix} u_{y} (1 - C_{\beta}) & -u_{x} (1 - C_{\beta}) & S_{\beta} \\ U^{2} & U^{2} & U \end{bmatrix}^{\top}$$

where  $U=\sqrt{u_x^2+u_y^2}$  (the magnitude of curvature),  $\beta=sU$  (the total bending angle at s), and  $C_\beta$  and  $S_\beta$  are symbols that represent  $\cos(\beta)$  and  $\sin(\beta)$  respectively. Note that (7) is written in terms of the Cartesian components of the curvature vector. This is equivalent to the commonly used constant-curvature transformation reviewed in [7] (which is expressed in terms of the polar angle and magnitude of the curvature vector) but (7) has the advantage that it does not suffer from an artificial singularity in the straight configuration which is inherent to the polar representation.

If m segments exist in series, the transformation at the tip of the robot is then

$$\mathbf{T}_{tip}(s) = \prod_{j=1}^{m} \mathbf{T}_{j}(l_{j})$$
 (8)

where  $l_j$  is the arc-length of the  $j^{th}$  segment. Note that in the case of a helical bellows pair, the overlapped section length changes as a function of actuation angles due to the helical pitch of the bellows, and there is an additional segment at the tip in which only one bellows is present (in which case (6) reduces to  $\mathbf{u} = \mathbf{R}(\theta_i)\mathbf{u}_i^*$ ). In the case of a pair of helical bellows tubes, the length of this additional segment  $l_2$  can be calculated as  $l_2 = h|\theta_2 - \theta_1|$  where  $\theta_2$  and  $\theta_1$  are the outer and inner bellows base angles (defined such that  $\theta_2 = \theta_1$  when the bellows are fully overlapped) and h is the helical pitch of the bellows design. Depending on the handedness of the helix, and the direction of base rotation, the tip segment could consist of either the inner bellows or the outer bellows.

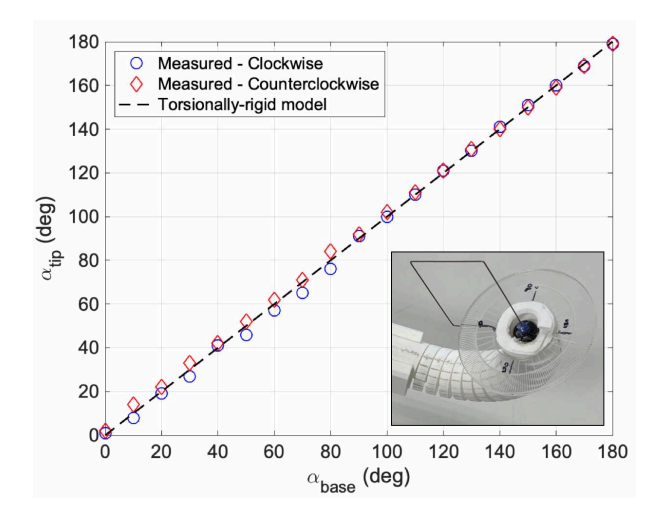


Fig. 6. The plot shows the angle between the inner and outer bellows at the tip over a range of relative base actuation angles. Torsional rigidity would imply the base and tip angles to be equal (dashed line). Thus the data confirms the torsionally rigid assumption of our model. The experimental setup is shown in the inset.

#### V. MODEL VALIDATION

In this section, we experimentally validate the model presented in Section IV and compare the accuracy of the parameters calibrated in Section III.

# A. Actuation Setup

We constructed a manual actuation system that enables rotation and translation of two concentric bellows as shown in Figure 5. The setup uses two rotary stages (Optics Focus MAR-60L-P) which allow independent rotation of each bellows base with a micrometer for fine angular adjustments with a readable resolution of 0.083°. Because helical bellows require simultaneous rotation and translation with a specific pitch, a single dovetail linear stage (Optics Focus MDX-4090-60) was used to allow relative translation as the tubes are rotated. The linear stage has a track range of 70 mm which is enough for our prototypes to provide multiple revolutions. As shown in Figure 5, the inner bellows attached to its rotary stage via a 1/8" diameter steel rod that passes through the outer bellows stage. The entire assembly is supported by a rigid acrylic frame.

# B. Validation of Torsionally Rigid Assumption

To validate our torsionally rigid model assumption (and the implication that friction does not affect the shape), we actuate the prototype over its entire workspace and measure the relative angle between the two bellows at the segment tip  $\alpha_{tip} = \theta_{2,tip} - \theta_{1,tip}$  and compare this value to the relative angle of the two bellows bases  $\alpha_{base} = \theta_{2,base} - \theta_{1,base}$ . If the bellows pair exhibits torsional rigidity with no loss to friction, the tip angle should equal the base angle for all base rotations.

The inner bellows rotates through  $180^{\circ}$  in both clockwise and counter clockwise directions in  $10^{\circ}$  increments. We use a graduated disk with a resolution of  $1^{\circ}$  attached at the distal tip of the outer bellows, and a wire pointer attached to the

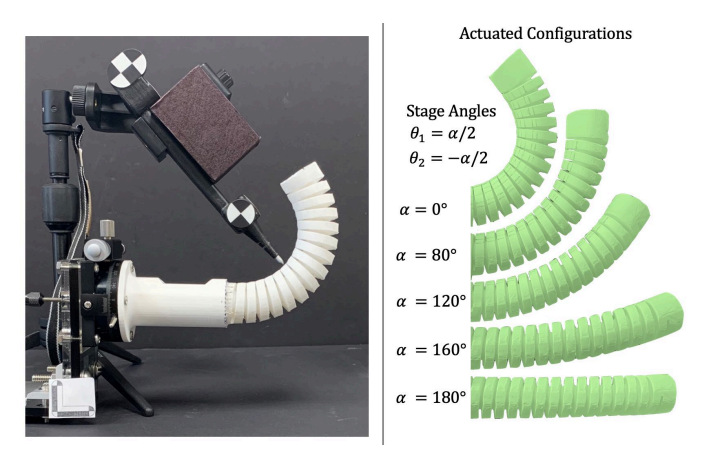


Fig. 7. Experimental setup for measuring points along the curvature of the bellows pair (left). The outer curvature of the bellows pair were measured in five configurations in which the angles of the inner and outer bellows were equal in magnitude but opposite in direction (right).

inner bellows to indicate angle readings. Figure 6 shows the experimental setup and the results of this experiment. The maximum difference between actuated and measured tip twist angle was only  $4^{\circ}$ , which confirms the assumptions of torsional rigidity and negligible frictional effects by exhibiting virtually zero torsional lag.

# C. Kinematic Model Validation

To validate the accuracy of the full kinematic model of Section IV, we actuate the bellows pair by equal angles in opposite directions (i.e.  $\theta_1=\alpha/2$ ,  $\theta_2=-\alpha/2$  for relative input angles ranging from  $\alpha=0^\circ$  (precurvatures aligned) to  $\alpha=180^\circ$  (precurvatures diametrically opposed) which actuates the bellows from maximum curvature, to almost completely straight as shown in Figure 7. The radii of precurvature for both bellows tubes are 0.055 m in the direction of side 1.

We used a stereoscopic camera (ClaroNav MicronTracker H3-60) along with a stylus pointer to measure points on the surface of the outer bellows. An adjustable desktop tripod with a camera mount attachment held the stylus pointer to provide reliable and steady measurements. We rigidly registered the camera frame to the robot base frame using a separate symmetric data set using MATLAB's pcregistericp() from the Camera Vision Toolbox. We evaluated the repeatability of the actuation and measurement procedure by recording the distal tip position of the bellows coming from both  $\alpha=0^{\circ}$  and from  $\alpha=180^{\circ}$  configurations for the  $\alpha=40^{\circ}, \alpha=60^{\circ}$  and  $\alpha=80^{\circ}$  cases. 10 individual tip positions were taken at each configuration, with 5 from each direction. The largest standard deviation of tip position for each configuration was 0.7 mm.

We compare the experimental surface shape data to predictions made by our kinematic model in Figure 7. Two different kinematic model predictions are shown: (1) using the flexural rigidities calibrated from FEA simulations, and (2) using the flexural rigidities calibrated experimentally (which are direction-dependent). The root mean square error (RMSE) for both models is tabulated in Table IV. The direction-dependent

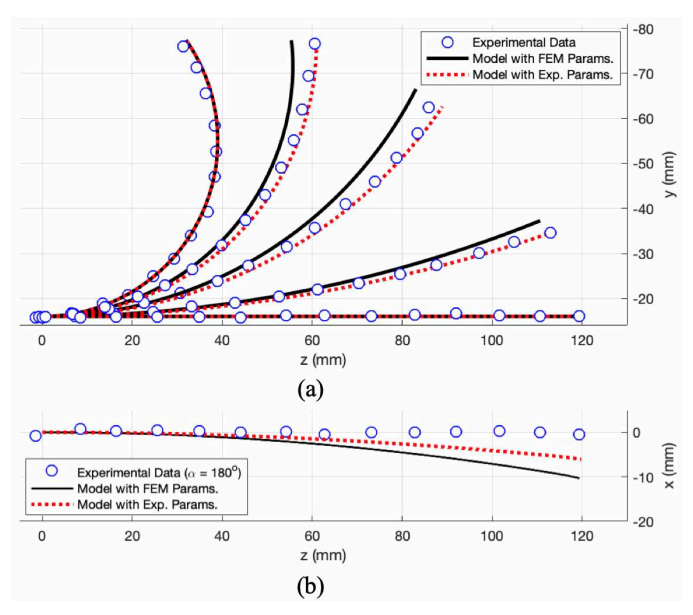


Fig. 8. Experimental measurements of helical bellows in actuated configurations in comparison with the torsionally-rigid kinematic model using FEA determined parameters and using experimentally determined parameters (a). (b) shows a side view of the out-of-plane error in the  $\alpha=180^{\circ}$  configuration.

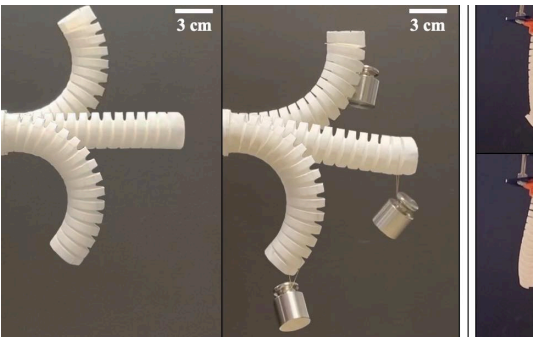
TABLE IV
KINEMATIC MODELING ERROR

	with FEA Param.	with Experimental Param.
Configuration	RMSE	RMSE
	(mm)	(mm)
$\alpha = 0^{\circ}$	1.28	1.28
$\alpha = 80^{\circ}$	2.30	1.12
$\alpha = 120^{\circ}$	3.89	1.99
$\alpha = 160^{\circ}$	4.28	2.72
$\alpha = 180^{\circ}$	4.27	2.78

experimental calibration of flexural rigidity in Section III improves shape prediction accuracy versus the FEA calibrated parameters. The shape validation results additionally verify the assumption of torsional rigidity and the implication that frictional forces, while present, do not significantly affect the shape because of the high stiffness of the torsional transmission.

# D. Discussion

These results demonstrate that concentric precurved bellows are feasible soft robot actuators. Whereas friction limits the kinematic accuracy and bending range of tendon/cable-driven continuum manipulators [23], [24], we demonstrated that a concentric-bellows strategy is largely unaffected by frictional forces at large bending angles due to the high torsional stiffness of the transmission. Fluid-driven and material-based actuation may entail other trade-offs in terms of actuation bandwidth and safety (e.g. high pressures). To demonstrate payload capacity (and further confirm that friction does not hinder performance), Figure 9 and the video attachment show a prototype lifting a 100g tip load, which is 4 times the mass of the bellows pair, while mostly retaining its desired shape across the bending range. Payload capacity can be tailored to the application by selecting the wall thickness and



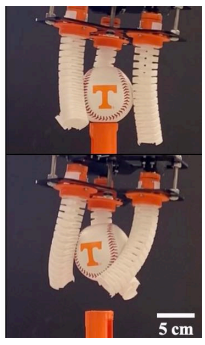


Fig. 9. Payload capacity of helical concentric precurved bellows pair actuated with and without 100g tip load (left) and a soft gripper demonstration (right).





Fig. 10. Nickel alloy bellows sample courtesy of Servometer. Bellows can be fabricated at scale suitable for minimally-invasive surgical applications (left) and retain large bending angles at this scale (right).

other dimensions of the convolution geometry. In general, increasing the wall thickness increases the effective EI while minimally affecting EI/GJ, thus increasing payload capacity while maintaining robot performance and overall diameter. For example, doubling the wall thickness of the outer helical bellows to 0.6 mm increases EI by a factor of 5 while only increasing EI/GJ by 25% to 0.05.

Applications of concentric-bellows actuation include manipulation tasks at scales appropriate for human cooperation. As a demonstration, we fabricated a soft gripper using revolute bellows fingers that can grasp and lift a baseball ( 150g, 75mm diameter) as shown in Figure 9 and the supplementary video. It is also feasible to use concentric bellows actuation in surgical tools that require a high amount of angulation. For example, Figure 10 demonstrates a 5 mm diameter bellows precisely fabricated by nickel electro-forming, courtesy of Servometer, which is capable of at least a  $\pm 135^{\circ}$  degree bending range.

# VI. CONCLUSIONS AND FUTURE WORK

We have presented initial work toward using precurved concentric bellows as soft robot actuators. This new actuation strategy exhibits good performance over large bending angles due to an EI/GJ ratio much lower than what prior strategies have exhibited, eliminating the issue of unstable snapping and allowing the use of constant-curvature kinematic models. Future work may include further miniaturization, multi-segment soft manipulators, and design optimization.

#### REFERENCES

[1] D. Drotman, S. Jadhav, M. Karimi, P. deZonia, and M. T. Tolley, "3D printed soft actuators for a legged robot capable of navigating unstruc-

- tured terrain," in 2017 IEEE International Conference on Robotics and Automation (ICRA). IEEE, 5 2017, pp. 5532–5538.
- [2] P. H. Nguyen, C. Sparks, S. G. Nuthi, N. M. Vale, and P. Polygerinos, "Soft Poly-Limbs: Toward a New Paradigm of Mobile Manipulation for Daily Living Tasks," *Soft Robotics*, vol. 6, no. 1, pp. 38–53, 2 2019.
- [3] R. F. Shepherd, F. Ilievski, W. Choi, S. A. Morin, A. A. Stokes, A. D. Mazzeo, X. Chen, M. Wang, and G. M. Whitesides, "Multigait soft robot." *Proceedings of the National Academy of Sciences of the United States of America*, vol. 108, no. 51, pp. 20400–3, 12 2011.
- [4] J. Burgner-Kahrs, D. C. Rucker, and H. Choset, "Continuum Robots for Medical Applications: A Survey," *IEEE Transactions on Robotics*, vol. 31, no. 6, pp. 1261–1280, 12 2015.
- [5] T. George Thuruthel, Y. Ansari, E. Falotico, and C. Laschi, "Control Strategies for Soft Robotic Manipulators: A Survey," *Soft Robotics*, vol. 5, no. 2, pp. 149–163, 4 2018.
- [6] D. Rus and M. T. Tolley, "Design, fabrication and control of soft robots," *Nature*, vol. 521, no. 7553, pp. 467–475, 5 2015.
- [7] R. J. Webster and B. A. Jones, "Design and kinematic modeling of constant curvature continuum robots: A review," *International Journal* of Robotics Research, 2010.
- [8] H. B. Gilbert, D. C. Rucker, and R. J. Webster III, "Concentric Tube Robots: The State of the Art and Future Directions." Springer, Cham, 2016, pp. 253–269.
- [9] F. Schmitt, O. Piccin, L. Barbé, and B. Bayle, "Soft Robots Manufacturing: A Review," Frontiers in Robotics and AI, vol. 5, p. 84, 7 2018.
- [10] T. K. Morimoto and A. M. Okamura, "Design of 3-D Printed Concentric Tube Robots," *IEEE Transactions on Robotics*, vol. 32, no. 6, pp. 1419– 1430, 12 2016.
- [11] R. Webster, J. Romano, and N. Cowan, "Mechanics of Precurved-Tube Continuum Robots," *IEEE Transactions on Robotics*, vol. 25, no. 1, pp. 67–78, 2 2009.
- [12] P. Dupont, J. Lock, B. Itkowitz, and E. Butler, "Design and Control of Concentric-Tube Robots," *IEEE Transactions on Robotics*, vol. 26, no. 2, pp. 209–225, 4 2010.
- [13] J. Lock and P. E. Dupont, "Friction modeling in concentric tube robots," in 2011 IEEE International Conference on Robotics and Automation. IEEE, 5 2011, pp. 1139–1146.
- [14] J. Ha, G. Fagogenis, and P. E. Dupont, "Modeling Tube Clearance and Bounding the Effect of Friction in Concentric Tube Robot Kinematics," *IEEE Transactions on Robotics*, vol. 35, no. 2, pp. 353–370, 4 2019.
- [15] J.-S. Kim, D.-Y. Lee, K. Kim, S. Kang, and K.-J. Cho, "Toward a solution to the snapping problem in a concentric-tube continuum robot: Grooved tubes with anisotropy," in 2014 IEEE International Conference on Robotics and Automation (ICRA). IEEE, 5 2014, pp. 5871–5876.
- [16] H. Azimian, P. Francis, T. Looi, and J. Drake, "Structurally-redesigned concentric-tube manipulators with improved stability," in 2014 IEEE/RSJ International Conference on Intelligent Robots and Systems. IEEE, 9 2014, pp. 2030–2035.
- [17] D.-Y. Lee, J. Kim, J.-S. Kim, C. Baek, G. Noh, D.-N. Kim, K. Kim, S. Kang, and K.-J. Cho, "Anisotropic Patterning to Reduce Instability of Concentric-Tube Robots," *IEEE Transactions on Robotics*, vol. 31, no. 6, pp. 1311–1323, 12 2015.
- [18] K. A. Xin Jue Luo, T. Looi, S. Sabetian, and J. Drake, "Designing Concentric Tube Manipulators for Stability Using Topology Optimization," in 2018 IEEE/RSJ International Conference on Intelligent Robots and Systems (IROS). IEEE, 10 2018, pp. 1764–1769.
- [19] L. Virgin, "On the flexural stiffness of 3D printer thermoplastic," International Journal of Mechanical Engineering Education, vol. 45, no. 1, pp. 59–75, 1 2017.
- [20] Ultimaker, "Technical data sheet Ultimaker PLA," Tech. Rep.
- [21] ASTM International, "ASTM D790-17 Standard Test Methods for Flexural Properties of Unreinforced and Reinforced Plastics and Electrical Insulating Materials," West Conshohocken, PA, 2017.
- [22] R. L. Bishop, "There is More than One Way to Frame a Curve," The American Mathematical Monthly, vol. 82, no. 3, p. 246, 3 1975.
- [23] G. Subramani and M. R. Zinn, "Tackling friction An analytical modeling approach to understanding friction in single tendon driven continuum manipulators," in *Proceedings - IEEE International Confer*ence on Robotics and Automation, vol. 2015-June, no. June. Institute of Electrical and Electronics Engineers Inc., 6 2015, pp. 610–617.
- [24] T. Kato, I. Okumura, S. E. Song, A. J. Golby, and N. Hata, "Tendon-Driven Continuum Robot for Endoscopic Surgery: Preclinical Development and Validation of a Tension Propagation Model," *IEEE/ASME Transactions on Mechatronics*, vol. 20, no. 5, pp. 2252–2263, 10 2015.